Scientia Iranica A (2013) 20(6), 1579–1594

Sharif University of Technology
Scientia Iranica
Transactions A: Civil Engineering
www.scientiairanica.com

Pulvino and peripheral joint effects on static and seismic safety of concrete arch dams

M.A. Hariri-Ardebili[a], H. Mirzabozorg[b,*] and M. Ghaemian[c]

a. *Department of Civil Environmental and Architectural Engineering, University of Colorado, Boulder, CO, USA.*
b. *Department of Civil Engineering, K.N. Toosi University of Technology, Tehran, Iran.*
c. *Department of Civil Engineering, Sharif University of Technology, Tehran, Iran.*

Received 23 October 2011; received in revised form 5 February 2013; accepted 25 June 2013

KEYWORDS
Contraction joints;
Arch dam;
Peripheral joint;
Pulvino;
Nonlinear seismic performance.

Abstract. One of the methods in limiting tensile stresses in arch dams and removing stress concentrations at the dam-foundation interface is setting the dam body on a concrete saddle called a Pulvino. In the present study, the effects of Pulvino and peripheral joints on the static behavior and seismic performance of arch dams are investigated. Dez Dam with a height of 203 m was selected as a case study and all contraction joints of the dam body were modeled using the discrete crack approach based on as-built drawings. Also, the surrounding rock was modeled as a mass-less medium tied to Pulvino. The dam-reservoir-foundation system was analyzed under static loads accounting for stage construction effects, hydrostatic and thermal loads. The provided numerical model was then excited using near- and far-field earthquake ground motion. It was found that modeling the peripheral joint between the saddle and the main dam body changes the direction of principal stresses and their distribution patterns, and the safety of the system is improved. In addition, over stressed surfaces on the faces of the dam body decreased in comparison with the model without a peripheral joint.

1. Introduction

Although concrete arch dams are regarded as safe structures during earthquakes, it is necessary to evaluate their seismic performance at various seismic levels. Mass concrete is brittle material and is susceptible to crack because of its low tensile strength. For construction facilities and in order to control tensile stress due to concrete shrinkage, temperature variations etc., arch dams are built as an assemblage of monoliths separated by vertical contraction joints [1]. Also, in some cases, peripheral joints are provided between the dam body and a concrete saddle called a Pulvino. Pulvino is utilized as an artificial footing for a dam body and causes a slender dam body by reducing the uncertainties of the foundation rock just beneath the body. In addition, using Pulvino in thin arch dams is a suitable method for constructing these kinds of dams in narrow gorges with strong foundation rock. Finally, a peripheral joint provided between Pulvino and the dam body is suitable for: Insuring symmetric stress and strain distribution within the dam body; decreasing probable tensile stresses in mass concrete; the suitable distribution of stresses in abutments and preventing severe stresses in these regions. In fact, modeling contraction and peripheral joints with the ability to partially open/close and also to slide may affect stress distribution and displacement patterns within the dam body under static loading and during seismic excitation.

*. *Corresponding author. Tel.: +98 21 88779623; Fax: +98 21 88779476*
E-mail addresses: mohammad.haririardebili@colorado.edu (M.A. Hariri-Ardebili), mirzabozorg@kntu.ac.ir (H. Mirzabozorg), ghaemian@sharif.edu (M. Ghaemian)

There is much research into the nonlinear seismic analysis of concrete arch dams which considers the contraction joint effect [1]. The monolith joint opening causes the release of tensile stresses in the arch direction and internal stresses are redistributed into the cantilever bending. Dowling and Hall [2] prescribed a discrete joint model represented by nonlinear springs for arch dams, taking into account the global opening and closing of vertical and horizontal joints. Fenves et al. [3] developed a nonlinear joint element and utilized a numerical analysis procedure for calculating the nonlinear seismic response of arch dams. Lau et al. [4] studied contraction joint and shear sliding effects on the response of arch dams. Also, Toyada et al. [5] studied joint opening effects by introducing a discrete spring as the joint and comparing analytical results with those obtained from experimental investigations.

It is noteworthy that there is no accessible numerical investigation into Pulvino and peripheral joint effects on the structural response of arch dams. Dolcetta et al. [6] studied the behavior of peripheral joints and their constructive aspects on arch dams. The peripheral joint was at first applied by Niccolai, and then Semenza [7] found a reliable procedure for it using a theoretical-experimental basis. The innovation was applied first to thin arch structures and then to arch-gravity ones. According to Dolcetta et al. [6], 84% of arch and arch-gravity dams in Italy built between 1939 (when the peripheral joint was present) and 1981 include the technique of peripheral joints. Table 1 reports some important arch dams built after 1960 with the peripheral joint.

Although there are no serious reports on arch dam failure due to peripheral joint effects, there is a failure report in reference [8] due to sliding in the upstream/downstream (US/DS) direction of the dam body sitting on its saddle. Based on this report, the Plum Dam, located in the Fujian Province in southeast China, was an experimental cylindrical arch dam with a height of 22 m and a crest length of about 72.6 m. The dam failed in September 1981, shortly after it was completed in May of the same year. Field investigations indicated that the failure occurred possibly due to upward and downstream sliding of the dam along its peripheral joint. The dam was built as a masonry structure composed of granite blocks in the main body, and included a peripheral joint between the dam and its artificial concrete abutment. The joint surfaces were coated with bitumen and polyvinyl chloride was used to seal the joint. Completed in May 1981, full storage of the reservoir was reached in June 1981. The dam was overtopped by 0.30 m over the crest on July, but no damage or unusual behavior was observed. In September, the dam ruptured spectacularly without any warning. Based on the field observations and detailed inspection of the failed dam, the following scenario was offered as the most probable mode of failure:

I. The body of the dam moved up along the peripheral joint, producing the first set of frictional traces parallel to the axis of the dam. The upward movement, in turn, caused widening of the horizontal arch spans, stressing the crown to the point of rupture.

II. The sudden failure of the structure was triggered by shearing of the top portion which did not include any joint.

III. The sudden release of pressure caused the water to rush through the rupture and allowed the material to fall back onto the peripheral joint, thus producing the second set of traces on the joint surface.

Table 1. Some of most important arch dams built in the world after 1960 with the peripheral joint and Pulvino technique.

Name	Country	Year	Height (m)	Crest length (m)
Dez	Iran	1963	203	240
La Soledad	Mexico	1962	92	137
Santa Rosa	Mexico	1963	117	135
El Novillo	Mexico	1964	140	190
Kawamata	Japan	1965	117	137
Paltinul	Romania	1972	108	460
Tachien	Taiwan	1974	180	290
Inguri	Georgia	1980	272	680

In the present study, the effects of Pulvino and peripheral joints on the static and seismic performance of a high concrete arch dam are investigated thoroughly for the first time, taking into account all the known nonlinearity sources. For this purpose, three different models were provided:

I. The dam body is simulated as a Linear Elastic Model called LEM for the material and none of the contraction or peripheral joints are modeled in this condition.

II. The dam body is modeled considering joint effects using a Discrete Crack Model approach (DCM), but materials are still linear elastic.

III. The dam body is modeled considering joint effects using a discrete crack model approach, and mass concrete nonlinearity is modeled using a smeared crack approach (DCM+SCM).

In both second and third mentioned models, all contraction joints are taken into account, but each model

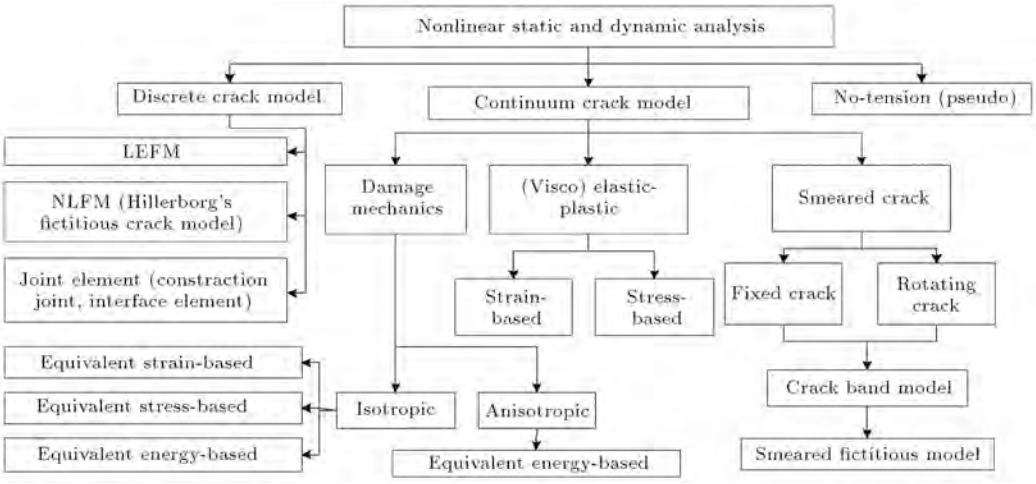

Figure 1. Different approaches in nonlinear analysis of arch dams.

is divided into two sub-models, only two of which have peripheral joints (illustrated by the letter "P"). So, there are four nonlinear models: DCM, DCM(P), DCM+SCM, and DCM+SCM(P).

In all cases, the applied loads are the dam body self weight, the hydrostatic pressure at Normal Water Levels (NWL) and thermal loads corresponding to the summer condition extracted from thermal analyses, including solar radiation effects. In addition, seismic loads based on near- and far-field ground motion are applied to the dam-reservoir-foundation system at a Maximum Credible Level (MCL).

2. Source of nonlinearity in concrete arch dams

Many fracture models have been developed for nonlinear analysis in two and three dimensions [9]. Figure 1 presents various methods for nonlinear static and dynamic analysis of concrete arch dams [10].

2.1. Discrete Crack Model (DCM)

In DCM, as a global approach, a crack is represented as a discrete gap along the inter-element boundary. The growth of cracks is governed by strength or fracture mechanic based constitutive models. The progressive physical discontinuity is reflected instantaneously in the finite element model by modifying the provided mesh [11,12]. It is generally argued that the nonlinear response of concrete dams is dominated by a few discrete long cracks.

In the present study, for modeling discrete crack, a special contact element is used, which is capable of modeling the contact between two adjacent nodes in the 3D domain. This contact element supports only compression in a normal direction to the joint plane, and also shears in the tangential direction. Figure 2 shows the flowchart used for calculating the relevant forces in the contact elements [13]. In this figure, $\vec{V}$

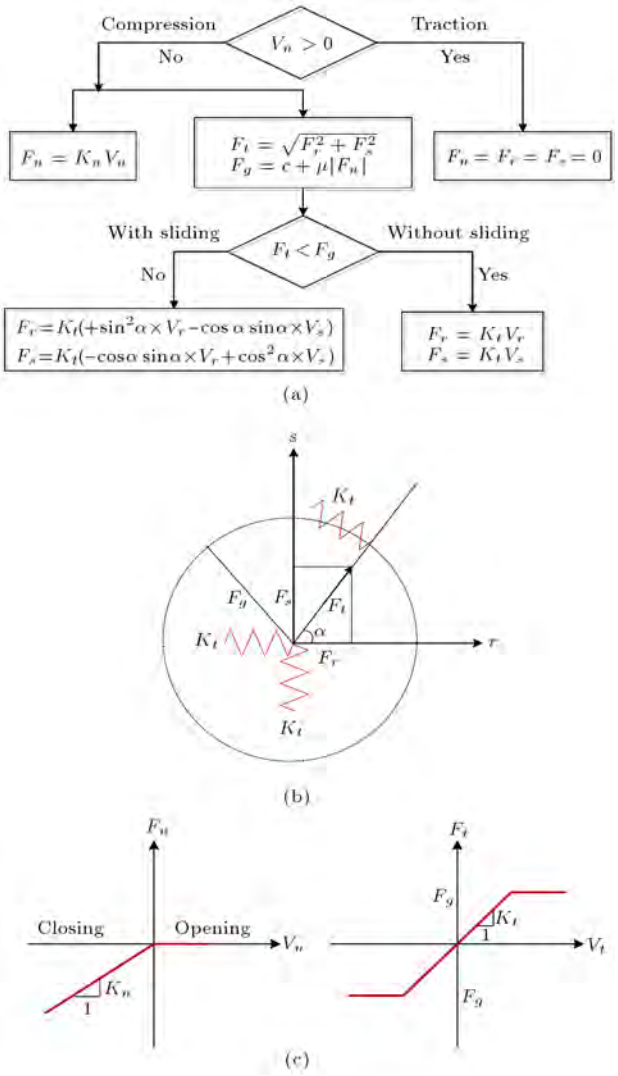

Figure 2. Details of 3D contact elements: (a) Flowchart for calculating force in joints; (b) schematic of contact element; and (c) force-deflection relations for joint opening/sliding.

is a vector representing the contact state, in which V_n indicates the state in the normal direction to the plane of the joint, and V_r and V_s indicate the state of the considered contact element in tangential directions.

Moreover, force-deflection relations for both the normal and tangential status are shown in the figure. In this flowchart, F_n, F_r and F_s are local components of the force vector; F_g is sliding force, F_t is shear force resultant in the joint, K_n and K_t are normal and tangential stiffness of the joint and 'a' is the angle between the two components of in-plane shear. As shown, the contact element cannot endure any tensile force or stress, but when it is in compression, it can suffer compression forces according to its normal stiffness coefficient and shear forces according to its tangential stiffness coefficient. When shear force resultant in the joint exceeds the joint sliding resisting force, the two nodes of the element begin sliding, with respect to each other, so that the joint sliding force is calculated using the Coulomb friction law. In Figure 2, c is cohesion factor and μ is friction coefficient, given as:

$$\mu = \tan(\varphi), \tag{1}$$

where φ is internal friction angle.

2.2. Continuum Crack Model (CCM)

One of the most important branches of CCM is the Smeared Crack Model (SCM) approach, which considers concrete nonlinear characteristics. These kinds of model must be capable of describing model constitutive behavior before and after cracking [14,15]. In this model, it is assumed that the concrete material is initially (before cracking) isotropic and linear until it reaches ultimate strength (Figure 3(a)), after which the elasticity modulus of the concrete is considered as average value E instead of linear actual E_0. During the pre-softening phase, stress increases linearly, along with an increase in strain. In this step, each reloading of elements leads to elastic returning of the strain. The stress-strain matrix is defined by Eq. (2), where v is the Poisson ratio.

$$[D_{\text{linear}}] = \frac{E}{(1+v)(1-2v)} \begin{bmatrix} (1-v) & v & v & 0 & 0 & 0 \\ v & (1-v) & v & 0 & 0 & 0 \\ v & v & (1-v) & 0 & 0 & 0 \\ 0 & 0 & 0 & \frac{1-2v}{2} & 0 & 0 \\ 0 & 0 & 0 & 0 & \frac{1-2v}{2} & 0 \\ 0 & 0 & 0 & 0 & 0 & \frac{1-2v}{2} \end{bmatrix}. \tag{2}$$

The tension failure of concrete is characterized by a gradual growth of cracks, which join together and finally disconnect larger parts of the structure. It is a usual assumption that forming cracks is a brittle process and the strength in the tension-loading direction abruptly goes to zero, after big cracks, or can be simulated with gradually decreasing strength, as shown in Figure 3(b). In this figure, E^s represents the secant modulus and f_t is the uniaxial tensile stress of mass concrete. Cracking occurs when principal tensile stress in any direction lies outside the failure surface. In this model, cracking is permitted in three orthogonal directions at each integration point. When cracking occurs at an integration point, the stress-strain relation is modified by defining a weak plane normal to the crack direction. Also, crushing occurs when all principal stresses are compressive and lie outside the failure surface. In this condition, the elastic modulus is set to zero in all directions. Based on the fact that the concrete has been cracked in one, two or three orthogonal directions, the stiffness matrix can be represented in the following forms:

I) Concrete has been cracked in one direction and the crack is open:

$$[D^{\text{open}}_{\text{cracked}}] = \frac{E}{1+v}$$

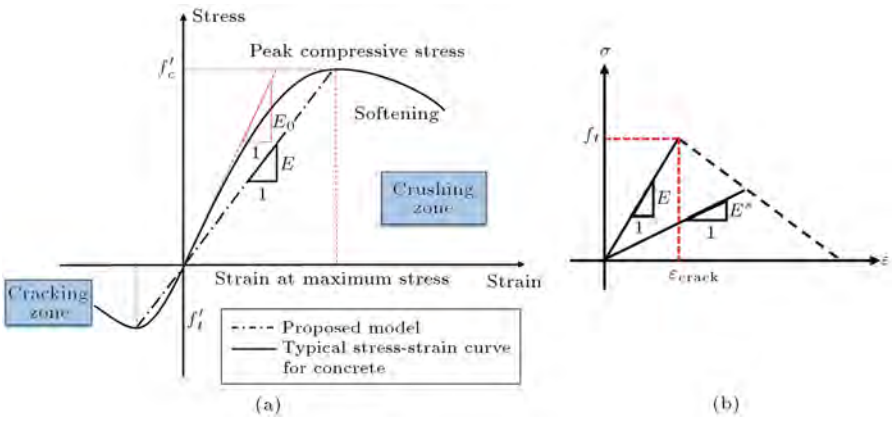

Figure 3. (a) Typical and simplified uniaxial compressive and tensile stress-strain curve for mass concrete. (b) Stress-strain relation for mass concrete in tension and its fracture.

$$\begin{bmatrix} \frac{E^S(1+v)}{E} & 0 & 0 & 0 & 0 & 0 \\ 0 & \frac{1}{1-v} & \frac{v}{1-v} & 0 & 0 & 0 \\ 0 & \frac{v}{1-v} & \frac{1}{1-v} & 0 & 0 & 0 \\ 0 & 0 & 0 & \frac{\beta_{\text{open}}}{2} & 0 & 0 \\ 0 & 0 & 0 & 0 & \frac{1}{2} & 0 \\ 0 & 0 & 0 & 0 & 0 & \frac{\beta_{\text{open}}}{2} \end{bmatrix}, \quad (3)$$

where, β_{open} is open shear transfer coefficient and defined as the factor that represents shear strength reduction across the cracked face.

II) Concrete has been cracked in one direction and the crack is closed (see Eq. (4) in Box I).

The shear transfer coefficient, β, represents conditions of the crack face. The value of β ranges from 0.0 to 1.0 with 0.0 representing smooth crack (complete loss of shear transfer) and 1.0 representing a rough crack (no loss of shear transfer).

III) Concrete has been cracked in two directions and the cracks are open:

$$[D^{\text{open}}_{\text{cracked}}] = E \begin{bmatrix} \frac{E^S}{E} & 0 & 0 & 0 & 0 & 0 \\ 0 & \frac{E^S}{E} & 0 & 0 & 0 & 0 \\ 0 & 0 & 1 & 0 & 0 & 0 \\ 0 & 0 & 0 & \frac{\beta_{\text{open}}}{2(1+v)} & 0 & 0 \\ 0 & 0 & 0 & 0 & \frac{\beta_{\text{open}}}{2(1+v)} & 0 \\ 0 & 0 & 0 & 0 & 0 & \frac{\beta_{\text{open}}}{2(1+v)} \end{bmatrix}. \quad (5)$$

IV) Concrete has been cracked in two directions and both cracks are closed (see Eq. (6) in Box II).

V) Concrete has been cracked in three directions and the cracks are open:

$$[D^{\text{open}}_{\text{cracked}}] = E \begin{bmatrix} \frac{E^S}{E} & 0 & 0 & 0 & 0 & 0 \\ 0 & \frac{E^S}{E} & 0 & 0 & 0 & 0 \\ 0 & 0 & \frac{E^S}{E} & 0 & 0 & 0 \\ 0 & 0 & 0 & \frac{\beta_{\text{open}}}{2(1+v)} & 0 & 0 \\ 0 & 0 & 0 & 0 & \frac{\beta_{\text{open}}}{2(1+v)} & 0 \\ 0 & 0 & 0 & 0 & 0 & \frac{\beta_{\text{open}}}{2(1+v)} \end{bmatrix}. \quad (7)$$

VI) Concrete has been cracked in three directions and all cracks are closed. In this situation, Eq. (6) can be written again. It should be noted that all the above stress-strain relations are written in a local coordinate system that is parallel to principal stress directions.

3. Numerical modeling of dam-reservoir-foundation system

Dez Dam is a 203 m high double curvature arch dam with a peripheral joint separating the dam body from Pulvino. The dam is located in a narrow gorge at the Dez River, in the Khuzestan Province in Iran. The dam was commissioned in 1963 and since then, sediments have accumulated within the reservoir up to an elevation of approximately 15 m below the intake of the power tunnel. General characteristics of the dam are summarized in Table 2.

At every level, the upstream face is configured using a constant radius arc, having s common center

$$[D^{\text{closed}}_{\text{cracked}}] = \frac{E}{(1+v)(1-2v)} \begin{bmatrix} (1-v) & v & v & 0 & 0 & 0 \\ v & (1-v) & v & 0 & 0 & 0 \\ v & v & (1-v) & 0 & 0 & 0 \\ 0 & 0 & 0 & \frac{\beta_{\text{close}}(1-2v)}{2} & 0 & 0 \\ 0 & 0 & 0 & 0 & \frac{1-2v}{2} & 0 \\ 0 & 0 & 0 & 0 & 0 & \frac{\beta_{\text{close}}(1-2v)}{2} \end{bmatrix}, \quad (4)$$

where β_{close} is closed shear transfer coefficient.

Box I.

$$[D^{\text{closed}}_{\text{cracked}}] = \frac{E}{(1+v)(1-2v)} \begin{bmatrix} (1-v) & v & v & 0 & 0 & 0 \\ v & (1-v) & v & 0 & 0 & 0 \\ v & v & (1-v) & 0 & 0 & 0 \\ 0 & 0 & 0 & \frac{\beta_{\text{close}}(1-2v)}{2} & 0 & 0 \\ 0 & 0 & 0 & 0 & \frac{\beta_{\text{close}}(1-2v)}{2} & 0 \\ 0 & 0 & 0 & 0 & 0 & \frac{\beta_{\text{close}}(1-2v)}{2} \end{bmatrix}. \quad (6)$$

Box II.

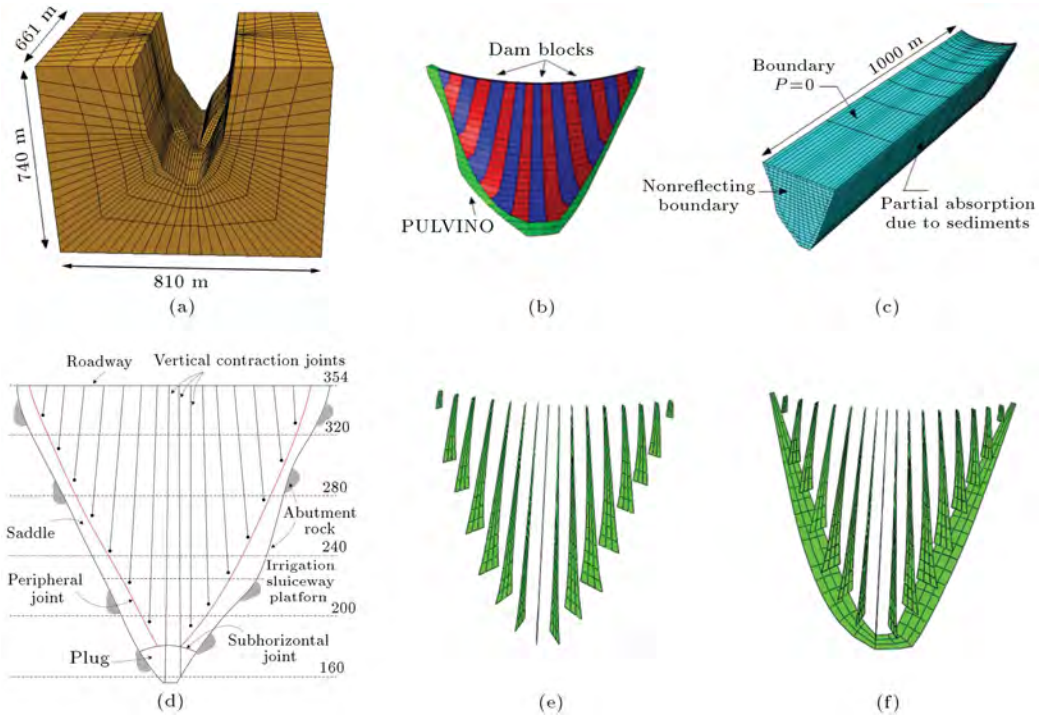

Figure 4. Finite element model of (a) foundation rock, (b) dam, and (c) reservoir. (d) Downstream view of Dez Dam and location of joints. (e) F.E. model of contraction joints (DCM and DCM+SCM models). (f) F.E. model of contraction and peripheral joints (DCM(P) and DCM+SCM(P) models).

Table 2. Main characteristics of Dez Dam.

Characteristics	Values
Maximum height above the foundation	203.5 m
Crest length	240 m
Crest thickness	4.5 m
Base thickness at body/Pulvino	21 m/28 m
Concrete volume (dam only)	328000 m^3
Concrete volume (dam and Pulvino)	142000 m^3
Crest height	354 m asl*
Normal operational level	350 m asl
Minimum operational level	290 m asl
Full reservoir capacity	3350 Mm^3

* Above sea level.

with another constant radius arc, forming the central portion of the downstream face. This configuration results in a constant thickness in the central portion at each level. Towards the abutments, the downstream face follows smaller radii arcs, thereby increasing the arch thickness approaching the abutments. The central angles of arches increase gradually from the roadway over the top of the dam body to approximately six-tenths of the top of the plug, which is located approximately nine-tenths of the distance down from the top of the roadway. The radii of the arches decrease from top to bottom. The centers of horizontal arches also move upstream. This results in a pronounced downstream overhang of the roadway in the central portion of the dam and a general concave appearance when viewed from downstream.

3.1. Finite element model

The finite element idealization provided for the dam, foundation rock and reservoir is presented in Figure 4(a) to (c). In the present study, two models were developed. The first model consists of 792 eight-node brick solid elements for modeling the concrete dam and Pulvino (which is used in LE and DCM models), and the second one consists of 6336 eight-node elements (which is used in DCM+SCM models). In addition, 3770 solid elements were used for modeling the foundation and finally, the reservoir was modeled using 3660 Eulerian fluid elements. Also, there are 784 contact elements in DCM and 1372 elements in SCM+DCM models, 956 contact elements in DCM(P) and 1673 elements in DCM+SCM(P) for modeling contraction and peripheral joints.

Figure 4(d) to (f) shows the location of contraction/peripheral joints in as-built drawings and also in the provided finite element model. K_n and K_s (normal and tangential stiffness in joints) are taken as 240 GPa/m and 24 GPa/m, respectively. Based on sensitivity analyses conducted by the authors, these stiffness coefficients lead to reasonable opening and sliding in contraction joints. Moreover, K_n and K_s for a peripheral joint are considered 210 GPa/m and 16.8 GPa/m, respectively [16].

Table 3. Material properties of the mass concrete and foundation rock.

Loading type	Mass concrete						Foundation		
	Isotropic elasticity	Poisson's ratio	Density	Thermal expansion coefficient	Compressive strength	Uniaxial tensile strength	Isotropic elasticity-saturated	Isotropic elasticity-unsaturated	Poisson's ratio
Static	40 GPa	0.2	2400 kg/m^3	6×10^{-6} 1/°C	35 MPa	3.4 MPa	13 GPa	15 GPa	0.25
Dynamic	46 GPa	0.14	2400 kg/m^3	6×10^{-6} 1/°C	36.6 MPa	5.1 MPa	13 GPa	15 GPa	0.25

Table 4. Characteristics of selected earthquake ground motions.

Ground motion and station	Loma Prieta, Gilroy array #1, CDMG station 47379 (near-field)			Landers, Silent Valley, CDMG station 12206 (far-field)		
Component (φ°)	**G01000**	G01090	G01-UP	SIL000	**SIL090**	SIL-UP
Abbreviation	NLP-00	NLP-90	NLP-UP	FLA-00	FLA-90	FLA-UP
PGA (g)	0.411	0.473	0.209	0.050	0.040	0.038
PGV (cm/s)	31.57	33.87	13.97	3.73	5.07	3.23
PGV/PGA (s)	0.078	0.073	0.068	0.076	0.129	0.086
Arias intensity (m/s)	1.055	1.679	0.296	0.074	0.069	0.052
M		6.9			7.3	
Ms		7.1			7.4	
R (km)		10.50			51.70	
Significant duration (s)	6.53	3.68 **9.00**	7.18	29.98	30.72 **31.00**	30.04

3.2. Material properties

Material properties for the mass concrete and foundation rock are described in Table 3 [17]. Furthermore, reservoir water density is 1000 kg/m^3, sound velocity is 1440 m/s in water and the wave reflection coefficient for the reservoir around the boundary is taken as 0.8, conservatively. At the far-end boundary of the reservoir, a viscous boundary is used to prevent wave reflection from this surface. Also, surface sloshing is neglected in the present case, and a zero pressure boundary condition is used for the reservoir free surface, which is an acceptable assumption in high dams [18,19]. It is noteworthy that all material properties were obtained based on calibration of the numerical model under static and thermal conditions using instruments and geodetic data [17].

4. Loading history

Applied loads on the model and their sequences are: the dam body self weight (considering ten stage construction), hydrostatic pressure (considering gradually impounding of reservoir water), thermal loads (based on summer condition obtained from thermal transient analysis of the dam [16]), and finally earthquake load. Sediment load was not considered in the current study due to its negligible effect on the structural response of high arch dams. The Newmark-β time-integration method was utilized to solve the coupled nonlinear problem of a dam-reservoir-foundation system. It is noteworthy that the displacement and flow characteristics were chosen as the convergence criteria in each load step of the conducted dynamic analyses.

For dynamic analyses, the system was excited using both near-field and far-field earthquake ground motions, scaled based on the design spectrum of the dam site at a Maximum Credible Level (MCL).

Characteristics of the selected ground motion are summarized in Table 4. Time-histories of the ground acceleration for both groups of ground motion, as well as a time interval of significant duration, are depicted in Figure 5. For specifying the significant duration of excitation, Arias intensity on a Husid diagram was used and then a time interval between 5% and 95% of Arias intensity, based on the Trifunac and Brady theory, was selected [20]. With this method, significant time duration for near-field ground motion is 9.00 s, while for far-field, is obtained to be 31.00 s. In addition, time-histories of ground velocity for the major direction of these ground motions are depicted in Figure 6. Considering that the main direction of arch dams is the stream direction, the major direction of ground motion was applied to the system in the stream direction [21]. Near-field ground motion was chosen in such a manner wherein its distance from the fault was about 10 km and also an apparent velocity pulse was evident in the velocity time-history (Figure 6) [22,23]. It is noteworthy that all three components of earthquake ground motion are applied to the dam-foundation-reservoir system, simultaneously. Figure 7 shows the

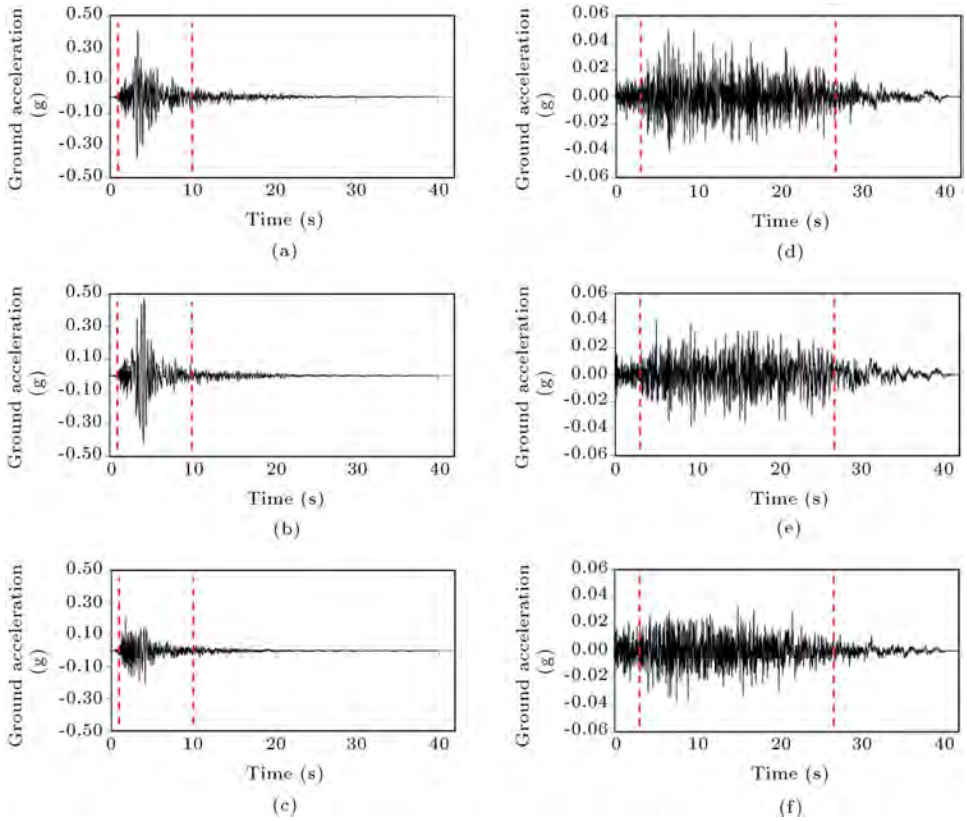

Figure 5. Ground acceleration time history for (a) NLP-00 (near-field major component), (b) NLP-90, (c) NLP-UP, (d) FLA-00, (e) FLA-90 (far-field major component) and (f) FLA-UP.

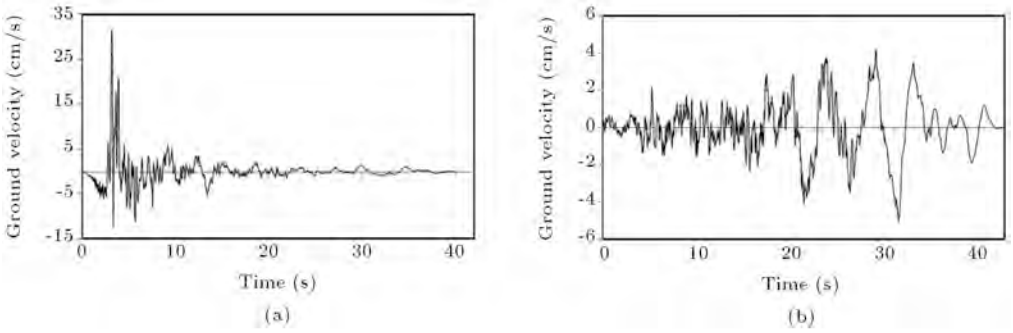

Figure 6. Ground velocity time history for (a) NLP-00 (near-field major component) and (b) FLA-90 (far-field major component).

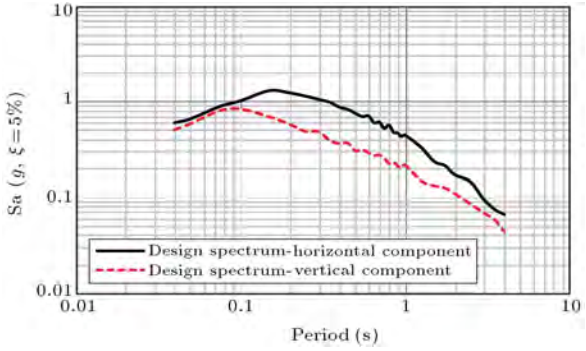

Figure 7. Horizontal and vertical components of acceleration design spectrum for Dez Dam site.

acceleration response spectrum, which was extracted based on hazard analysis of the Dez Dam site. Also, structural damping was taken as 5% of critical damping in all models, and the Rayleigh damping method was utilized to determine the mass and stiffness proportional damping coefficients, α_M and β_K, respectively.

5. Results and discussion

5.1. Modal analysis

Figure 8 compares the natural vibration periods extracted from LEM, DCM and DCM(P). As can be seen, after the 15th mode, the three models give the

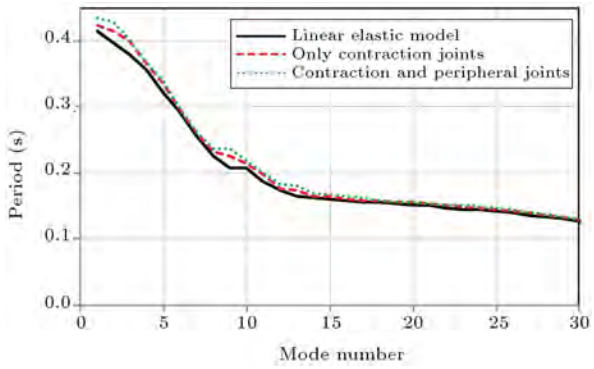

Figure 8. Coupled system periods in first 30 modes.

same period. However, in lower modes, there are some differences. LEM gives the smallest period of vibration and DCM(P) has the largest, which is logical due to joint effects on the stiffness of the structure. In fact, DCM is a little softer than LEM, and DCM(P) is softer than DCM, due to its peripheral joint. It should mention that the current approach for the modal analysis of a coupled system only considers the initial reduction in stiffness due to modeling the weak planes as joints in the dam, and neglects secondary stiffness reduction due to deformation. The period of the first mode in DCM(P) is 0.434 s, in DCM is 0.422 and in LEM is 0.414 s, respectively.

5.2. Seismic performance evaluation

The seismic performance of concrete arch dams is evaluated considering displacements, stresses, Demand-Capacity Ratio (DCR), Cumulative Inelastic Duration (CID) and spatial extension of overstressed areas on US and DS faces of the dam body. In the current section, some of these indices are considered in detail [24,25]. For arch dams, DCR refers to the ratio of the calculated arch or cantilever stress to the tensile strength of mass concrete, but it can also be developed for the principal stresses [25]. The maximum permitted DCR extracted from linear analysis is 2.0. This corresponds to a stress demand twice the tensile strength of mass concrete. Cumulative inelastic or overstress duration refers to the total duration of stress excursions above a stress level associated with a certain DCR. For assessing the probable level of damage, cumulative inelastic duration is utilized in conjunction with DCR. Time-histories of the most critical nodes within the dam body are shown in Figure 9(a) and (b). Moreover, the performance curves for the mentioned critical nodes and Performance Threshold Curve (PTC) proposed by Ghanaat [26] are depicted in Figure 9(c). As can be seen, for both near- and far-field ground motions, performance curves exceed PTC, but are more severe for far-field ground motion. In addition, the locations of three performance zones are shown in this figure.

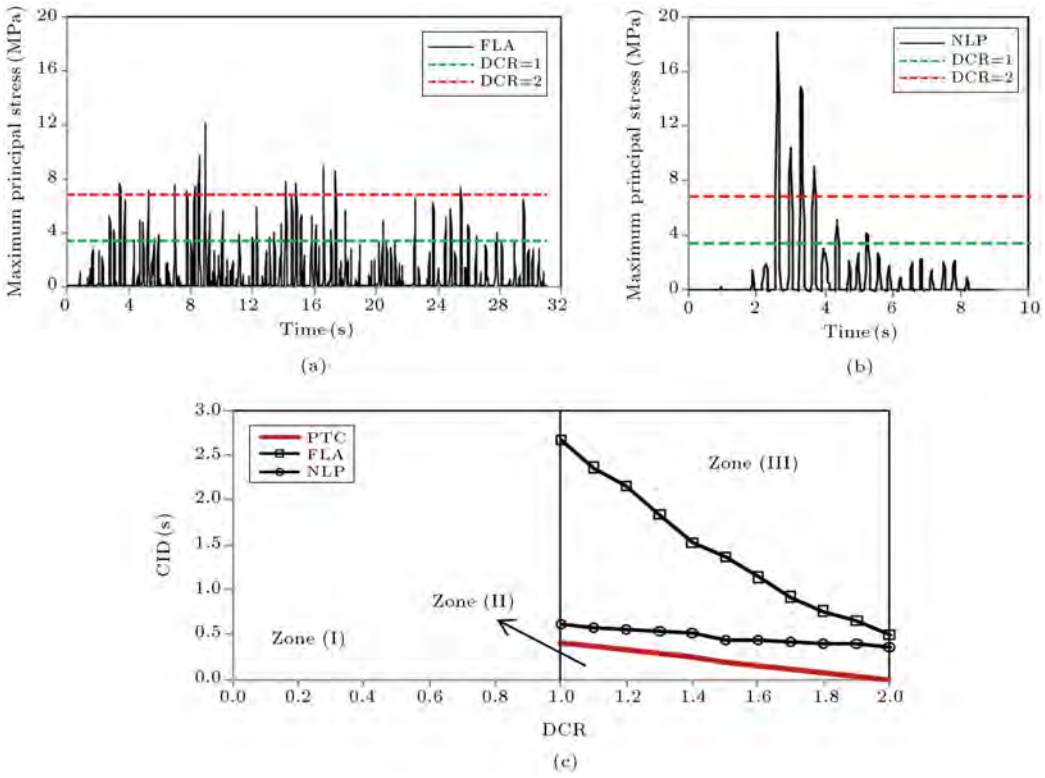

Figure 9. Time-history of maximum first principal stress for the most critical node within the dam body under (a) far-field ground motion, (b) near-field ground motion, and (c) performance curves for the most critical nodes in near- and far-field ground motions.

Figure 10. Overstressed area on the upstream/downstream faces of the dam body: (a) Far-field ground motion; and (b) Near-field ground motion.

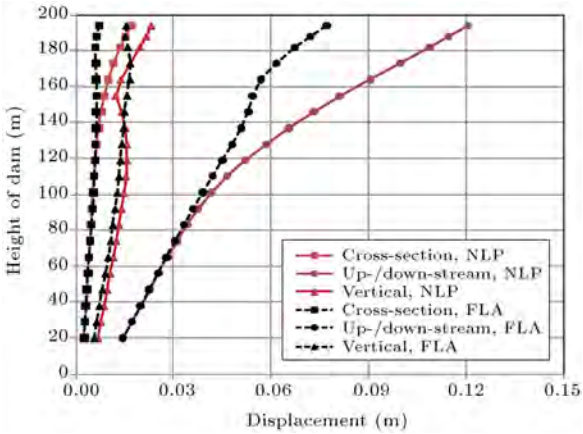

Figure 11. Non-concurrent envelope of displacement in cross-section, up-/down-stream and vertical direction for far-field and near-field ground motions.

In addition to the foregoing performance criteria, the proposed damage criteria are require to be bounded in small regions, so that the evaluation on the basis of LEM is still valid. If the spatial extent of damage or nonlinear response is limited to 20% of total areas on US or DS faces, the LEM is valid [25]. Figure 10 shows the spatial extension of overstressed areas on the US/DS faces of the dam body. Finally, the noncurrent displacement envelope for upstream nodes of the central cantilever is depicted in Figure 11. After analyzing the dam-reservoir-foundation system and extracting the required results, the performance of the dam based on LEM is interpreted utilizing the pointed out criteria and the flowchart presented in Figure 12 [25].

5.3. Peripheral joint effects

5.3.1. Displacement and joint behavior

Figure 13 shows the displacement time-history of the crest mid-point in the stream direction extracted from

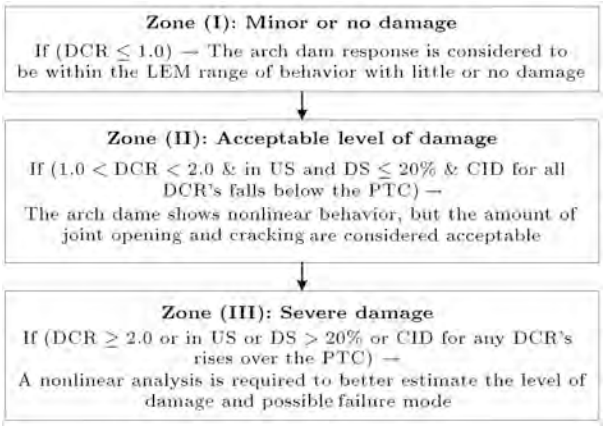

Figure 12. Interpretation of results for seismic performance evaluation based on LEM.

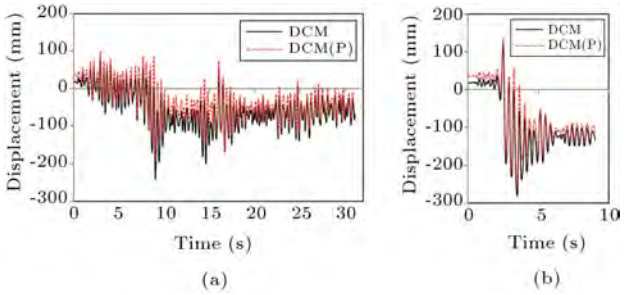

Figure 13. Time-history of the crest displacement in the stream direction extracted from DCM and DCM(P) models: (a) Far-field ground motion; and (b) near-field ground motion.

DCM and DCM(P) models. It should be noted that at each location, there are two points at the left and right block. For example, points A and A′ are both on the crown cantilever at the same location; the first one is on the left block and the second point is on the right one. In this section, only time-histories of the point at the left-side block are considered (point A). Table 5 summarizes the extreme values of displacement extracted from graphs on Figure 13. As can be seen, the static displacement for DCM on the crest mid-point is 17.8 mm and for DCM(P) this value reaches 34.3 mm, which is about twice the first one. It seems that crest static displacement increases in DCM(P) in comparison with DCM, which is related to the structural effect of the peripheral joint provided between the dam body and Pulvino. Under seismic conditions, modeling the

Table 5. Displacement values in static and dynamic conditions extracted from DCM and DCM(P) models.

Static and thermal analysis		Seismic analysis (far-field)		Seismic analysis (near-field)	
DCM	DCM(P)	DCM	DCM(P)	DCM	DCM(P)
+17.8 mm*	+34.3 mm	+82.9 mm	+97.8 mm	+119.2 mm	135.5 mm
		-239.9 mm**	-191.1 mm	-279.4 mm	-249.9 mm

* Positive sign means displacement in the downstream direction;

** Minus sign means displacement in the upstream direction.

peripheral joint leads to shifting the crest midpoint toward the downstream with a value that is about the difference in displacement of the two models in the static condition, while a decrease of movement in the upstream direction, which is about twice the pointed value, can be observed. In addition, Figure 14 shows a displacement envelope in the stream direction with and without considering peripheral joint effects for left-side and right-side blocks in the central area of the dam. Based on this figure, modeling the peripheral joint leads to decreasing maximum displacement in the upper quarter of the dam height, increasing displacement in the second upper quarter of the dam height, and there is almost no effect in the lower half of the dam height.

Figure 15 shows the envelope of the joint opening/sliding along the central cantilever under static and seismic loading conditions. Based on Figure 15(a), in static condition, the peripheral joint has no effect on the joint opening in the central block. The maximum joint opening is about 0.5 mm in central parts of the dam height.

Also, it reduces joint sliding in the upper 2/3 part of the body, so that this reduction reaches about 0.5 mm. Anyway, its effects on the central block joint behavior are negligible. Under seismic conditions (Figure 15(b) and (c)), it has almost no effect on the joint opening for the case with far-field ground motion, while it increases the opening for the upper 1/6 of the dam height, except in the crest point at which the joint opening decreases. In addition, the peripheral joint leads to a reduction in joint sliding in both cases at the upper half of the dam body. The joint sliding experienced by the crest point in the model excited using the far-field ground motion, with and without considering a peripheral joint, are 14 mm and 30 mm, respectively.

Figure 16 shows the envelope of the joint opening/sliding along the crest on the upstream face under static and seismic conditions. Based on Figure 16(a),

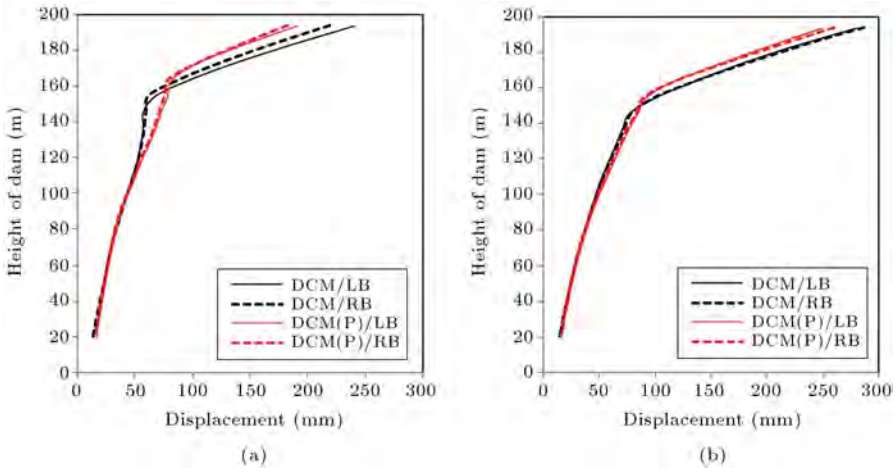

Figure 14. Non-concurrent envelope of displacement in up-/down-stream direction: (a) Far-field, and (b) near-field ground motions, in left-side block (LB) and right-side block (RB) of the center line .

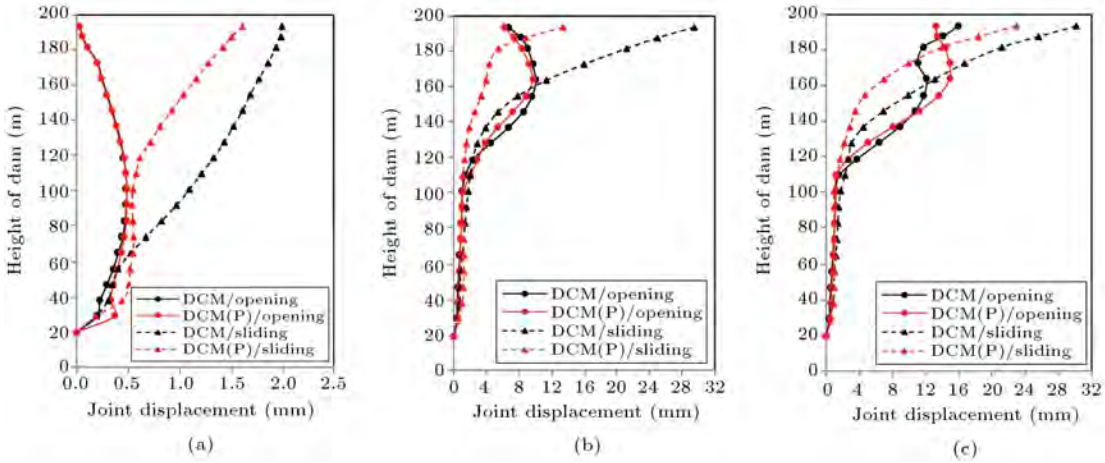

Figure 15. Envelope of joint opening/sliding in central block: (a) Static loading; (b) far-field ground motion; and (c) near-field ground motion.

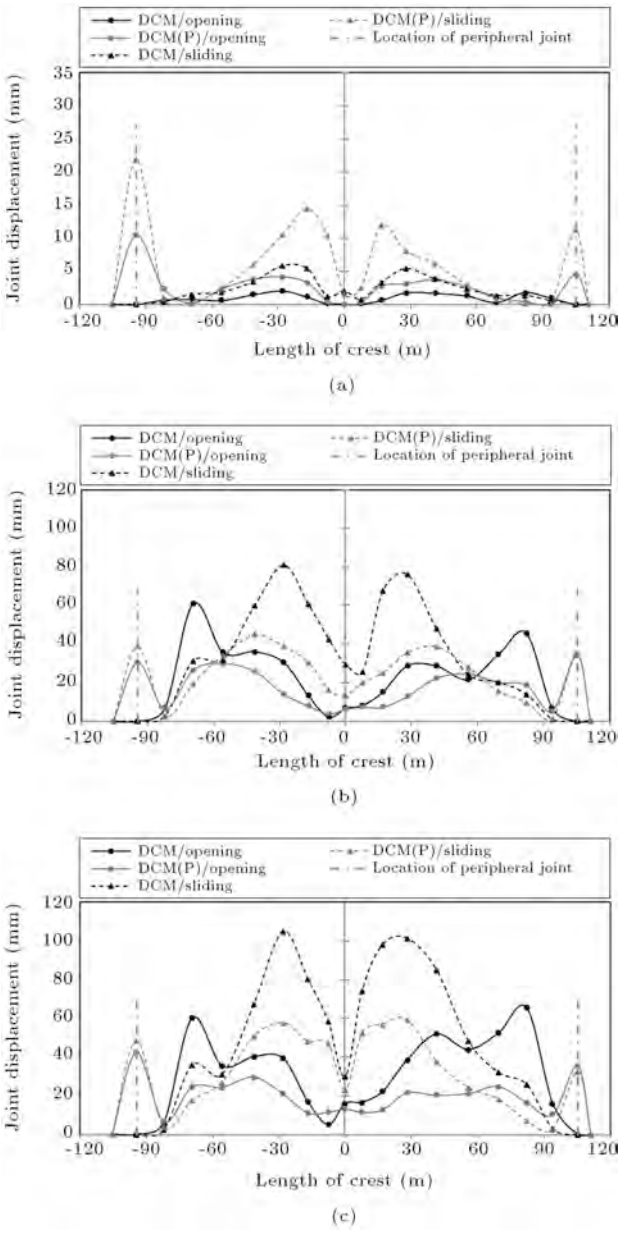

Figure 16. Envelope of joint opening/sliding along the crest length: (a) Static condition; (b) far-field ground motion; and (c) near-field ground motion.

by moving from the center to the corners, modeling the peripheral joints leads to an increase in both joint opening and sliding. On the other hand, the peripheral joint experiences notable opening/sliding at the crest level. At the left abutment, joint opening and sliding are 11 mm and 22 mm, respectively, while at the right abutment, they are 4.5 mm and 10.5 mm. Therefore, it can be concluded that under static conditions, modeling the peripheral joint leads to an undesirable response in joint behavior, but results are still in an acceptable range. In spite of the peripheral joint effect under a static condition, providing the peripheral joint is an effective method for reducing joint opening/sliding within the dam body, especially at the crest level, when the system is excited dynamically. As can be seen in Figure 16(b) and (c), crest points experience joint sliding about 81 mm under far-field conditions and about 105 mm under near-field ground motion conditions, while by modeling the peripheral joint, these values reach 44.5 mm and 57.5 mm, respectively. In addition, the joint opening in DCM for both types of ground motion is about 60.5 mm, while its value in DCM(P), utilizing far-field and near-field ground motion, is 38.8 mm and 48.5 mm, respectively. Joint opening in the left abutment raises from 11 mm under static condition to about 38.8 mm and 48.5 mm for cases with far- and near-field ground motion in the DCM(P) model. These values for the right abutment are 4.5 mm, 34.3 mm and 35.5 mm, respectively. The same results can be concluded for joint sliding in abutments. Generally, it can be concluded that modeling the peripheral joint leads to better behavior of joints, shear keys and the dam body under seismic loads for both far- and near-field ground motion mechanisms.

5.3.2. Distribution of principal stresses

Figure 17 represents the envelope of the first and the third principal stresses resulted from static and thermal analyses on US and DS faces of the dam body. As can be seen, the general patterns of the stress distributions are similar in DCM and DCM(P). The maximum first principal stress (which can be interpreted as tensile stress in the present case) is 5.43 MPa for DCM and 3.21 MPa for DCM(P). It means that modeling the peripheral joint reduces tensile stress under static condition about 41%, and increases the safety of the dam, meaningfully. Figures 18 and 19 show the non-concurrent envelope of the principal stresses extracted from the models excited using far-field and near-field ground motion. Like the static condition, the stress envelopes resulted from DCM and DCM(P) are similar, but, in both far- and near-field ground motion, modeling the peripheral joint leads to decreasing maximum tensile and minimum compression stresses. Under FLA ground motion, modeling the peripheral joint decreases S1 from 15.99 MPa to 14.87 MPa and, also decreases S3 from 35.44 MPa to 34.13 MPa, respectively. In fact, it leads to a reduction in S1 to about 7% and in S3 to about 3.7%. In addition, under NLP ground motion, modeling the peripheral joint decreases S1 from 21.06 MPa to 20.12 MPa and, also, decreases S3 from 44.60 MPa to 40.43 MPa, respectively. This leads to stress reduction to about 4.5% for S1 and 9.3% for S3. Obviously, although modeling the peripheral joint leads to decreasing total principal stresses, under both static and dynamic conditions, its main application is the redistribution and reduction of tensile stresses under a normal operational regime under static conditions.

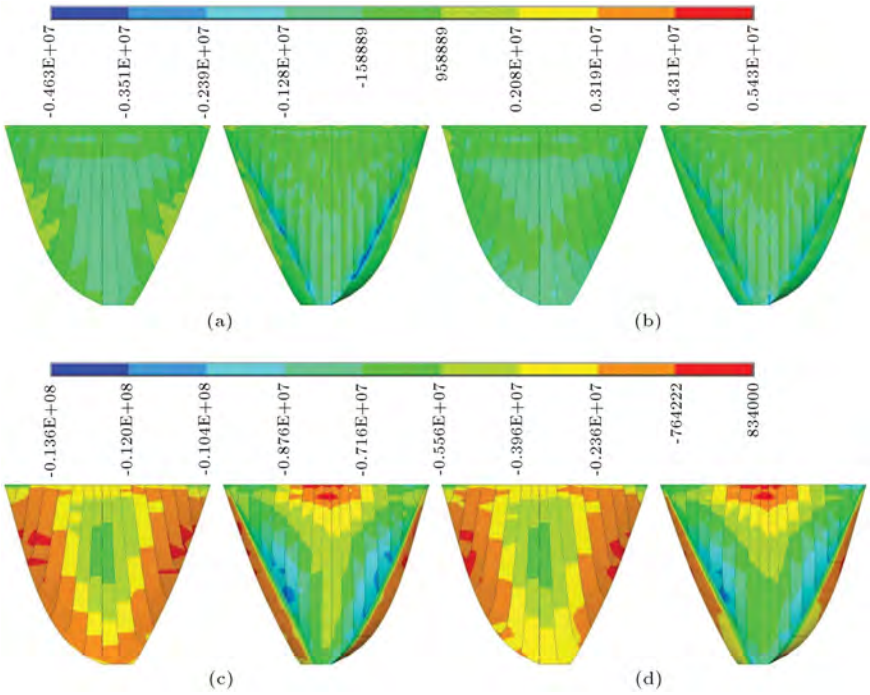

Figure 17. Static envelope of the principal stresses within the dam body: (a) S1-DCM; (b) S1-DCM(P); (c) S3-DCM; and (d) S3-DCM(P).

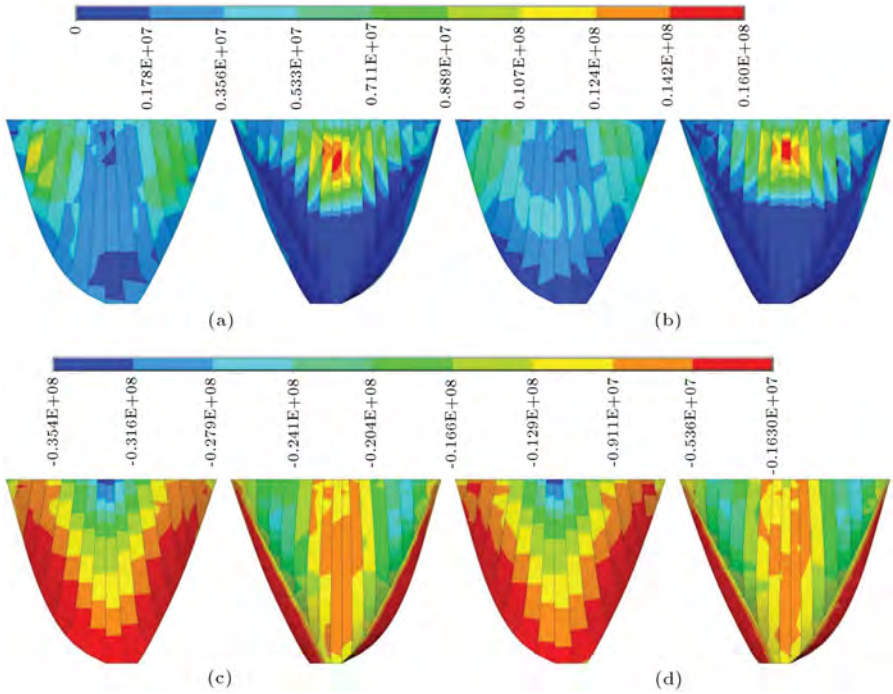

Figure 18. Non-concurrent envelope of the principal stresses within the dam body in the cases excited using the far-field ground motion: (a) S1-DCM; (b) S1-DCM(P); (c) S3-DCM; and (d) S3-DCM(P).

5.3.3. Damage in the dam body

In the present section, the crack profiles resulted from material nonlinearity under far- and near-field ground motions are studied, and the effect of peripheral joints in the propagation of cracks within the dam body is investigated. The values of the shear transfer coefficient for cracked sections under open and closed conditions were assumed to be 0.1 and 0.9, respectively, which is close to the results of the variable shear transfer coefficient using a co-axial rotating smeared crack model [27]. For this purpose, a new finite element model was developed in which the number of

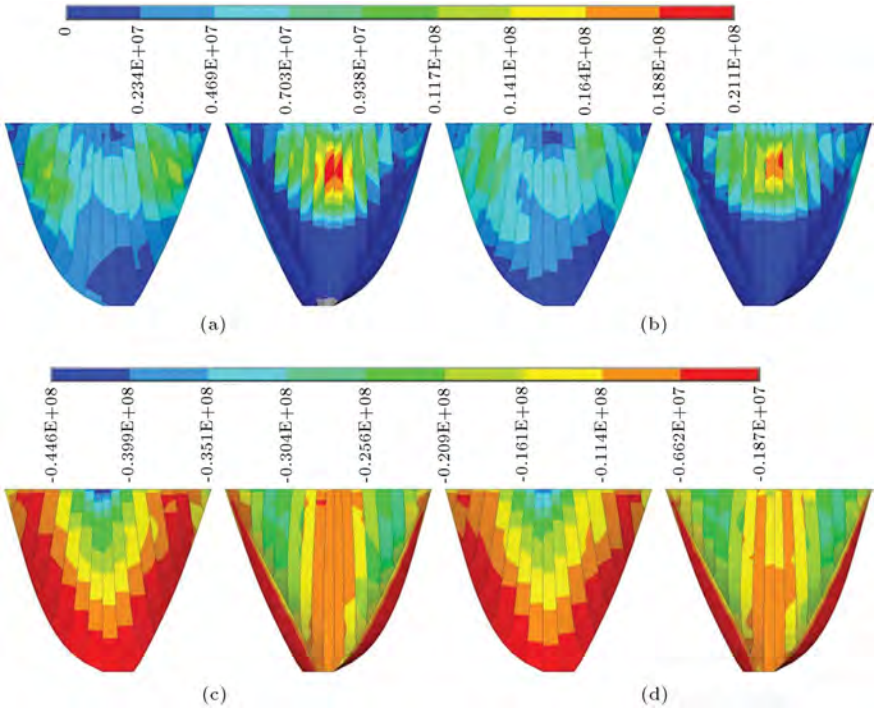

Figure 19. Non-concurrent envelope of the principal stresses within the dam body resulted from the model excited using the near-field ground motion: (a) S1-DCM; (b) S1-DCM(P); (c) S3-DCM; and (d) S3-DCM(P).

dam body elements were increased from 792 to 6336 elements. In the new set of models (DCM+SCM), the dam body has six layers of elements through the thickness and, so, crack propagation can be traced with high accuracy. In the new model, all contraction and peripheral joints are modeled as the previous one, except that the number of contact elements increases. As mentioned before, the elements can be cracked at each Gaussian point in the three orthogonal directions, corresponding to the three principal stress directions. In the present study, the First Crack (FC) in the Gaussian point is shown in red, the Second Crack (SC) is shown in green and the Third Crack (TC) is shown in blue, corresponding to the first, second and third principal stress directions at each Gaussian point. The existence of the blue Gaussian point in the crack profile shows that the considered point is cracked in all three directions and must be eliminated completely from the stiffness matrix contribution of the element. Crack profiles resulted from analyses utilizing far- and near-field ground motions are shown in Figures 20 and 21. As can be found, cracked elements are less in DCM+SCM(P) in comparison with DCM+SCM models in both cases. In the case of far-field ground motion, the crack profile resulted by modeling the peripheral joint is almost a subset of that in the DCM+SCM model, while under near-field ground motion, the crack profiles resulted from the two models show some differences. Modeling the peripheral joint can lead to a release of high tensile stresses on the interface of the dam-Pulvino and, therefore, reduces cracked elements near the abutments.

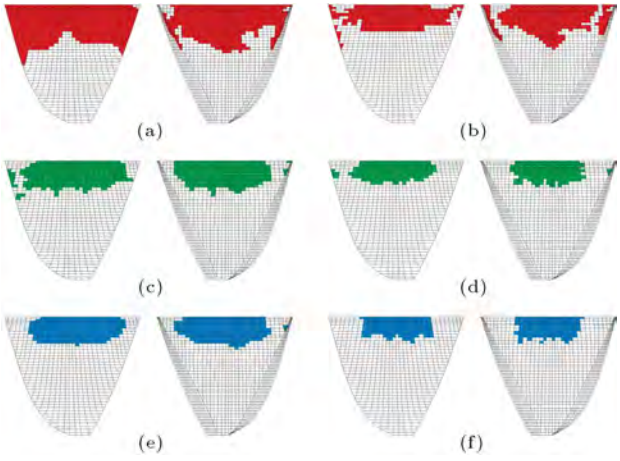

Figure 20. Crack profiles on US and DS faces of the dam body resulted from far-field ground motion:
(a) FC-DCM+SCM; (b) FC-DCM+SCM(P);
(c) SC-DCM+SCM; (d) SC-DCM+SCM(P);
(e) TC-DCM+SCM; and (f) TC-DCM+SCM(P).

6. Conclusion

In the present paper, the effect of Pulvino and a peripheral joint on the static and seismic behavior of high arch dams is considered. The Dez dam in Iran was chosen as a case study, and its struc-

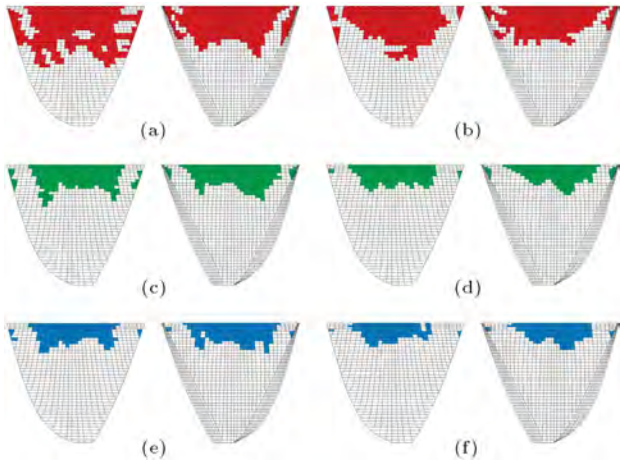

Figure 21. Crack profiles on US and DS faces of the dam body resulted from near-field ground motion:
(a) FC-DCM+SCM; (b) FC-DCM+SCM(P);
(c) SC-DCM+SCM; (d) SC-DCM+SCM(P);
(e) TC-DCM+SCM; and (f) TC-DCM+SCM(P).

tural behavior, due to summer conditions (including solar radiation effects) and near/far-field earthquake ground motion, was studied. Three basic models were prepared; LEM, DCM/DCM(P) and DCM+SCM/ DCM+SCM(P). Before nonlinear seismic analyses, a set of linear analyses were conducted on the model and the necessity for nonlinear analyses was investigated, based on the performance evaluation of the linear model using parameters like demand-capacity ratio, cumulative inelastic duration and extension of overstressed areas, on both upstream and downstream faces of the dam body. Subsequently, joint nonlinearity analyses were conducted by considering contraction joints in all models, while in some of them, the peripheral joint was modeled. It is noteworthy that all the dam body and joint grouting were modeled considering construction staging effects, as reported in as-built drawings. Based on the results, it was found that modeling the peripheral joint between the dam body and Pulvino causes a change in crest displacement. In addition, there are some changes in the patterns of tensile and compressive stress distribution and also, in the value of extremes. Moreover, the number of cracked elements in DSM+SCM(P) is less than that in DCM+SCM. Generally, it can be concluded that modeling a peripheral joint improves the safety margin of the dam-reservoir-foundation system under static conditions and under low seismic hazard levels considerably, while it has less effect on higher seismic hazard levels, such as the maximum credible level.

References

1. Zhang,C., Xu, Y., Wang, G. and Jin, F."Non-linear seismic response of arch dams with contraction joint opening and joint reinforcements", *Earthquake Engineering & Structural Dynamics*, **29**, pp. 1547-1566 (2000).
2. Dowling, M.J. and Hall, J.F. "Nonlinear seismic analysis of arch dams", *ASCE Journal of Engineering Mechanics*, **115**(4), pp. 768-789 (1989).
3. Fenves, G.L., Mojtahedi, S. and Reimer, R.B. "Effect of contraction joints on earthquake response of an arch dams", *Journal of Structural Engineering*, **118**, pp. 1039-1055 (1992).
4. Lau, D.T., Noruziaan, B. and Razaqpur, A.G. "Modelling of contraction joint and shear sliding effects on earthquake response of arch dams", *Earthquake Engineering & Structural Dynamics*, **27**, pp. 1013-1029 (1998).
5. Toyoda, Y., Ueda, M. and Shiojiri, H. "Study of joint opening effects on the dynamic response of an existing arch dam", *The 15th ASCE Engineering Mechanics Conference*, Colombia University, New York (2002).
6. Dolcetta, M., Marazio, A. and Bavestrello, F. "The peripheral joint at the arch dams: Design, behavior and constructive aspects", *The 39th Geomechanic-Colloquy Conference*, Salzburg (1990).
7. Semenza, C. "Arch dams - development in Italy", *Proceedings of the ASCE*, **82**, Paper 1017, pp. 1-42 (1956).
8. U.S. Army Corps of Engineering "EM-1110-2-2201: arch dam design", Washington D.C. (1994).
9. Mirzabozorg, H., Kianoush, R. and Jalalzadeh, B. "Damage mechanics approach and modeling non-uniform cracking within finite elements for safety evaluation of concrete dams in 3D space", *Structural Engineering and Mechanics*, **33**(1), pp. 31-46 (2009).
10. Mirzabozorg, H., Khaloo, A.R., Ghaemian, M. and Jalalzadeh, B. "Non-uniform cracking in smeared crack approach for seismic analysis of concrete dams in 3D space", *International Journal of Earthquake Engineering and Engineering Seismology*, **2**, pp. 48-57 (2007).
11. Hall, J.F. and Dowling, M.J. "Response of jointed arches to earthquake excitation", *Earthquake Engineering and Structural Dynamics*, **13**, pp. 779-798 (1985).
12. Goodman, R.E., Taylor, R.L. and Brekke, T.L. "A model for the mechanics of jointed rocks", *Journal of Soil Mechanics and Foundation Division ASCE*, **120**(4), pp. 1255-1271 (1994).
13. Azmi, M. and Paulte, P. "Three-dimensional analysis of concrete dams including contraction joint nonlinearity", *Engineering Structures*, **24**, pp. 757-771 (2002).
14. Gunn, R.M. "Non-linear design and safety analysis of arch dams using damage mechanics- Part I: formulation", *Hydropower & Dams*, **2**, pp. 67-74 (2001).
15. Hariri-Ardebili, M.A. and Mirzabozorg, H. "Seismic performance evaluation and analysis of major arch

dams considering material and joint nonlinearity effects", ISRN Civil Engineering, Article ID 681350, 10 pages (2012).

16. Hariri-Ardebili, M.A., Mirzabozorg, H., Ghaemian, M., Akhavan, M. and Amini, R. "Calibration of 3D FE model of Dez high arch dam in thermal and static conditions using instruments and site observation", *Proceedings of the 6th International Conference in Dam Engineering*, Lisbon, Portugal (2011).

17. Hariri-Ardebili, M.A. and Mirzabozorg, H. "Feasibility study of Dez arch dam heightening based on nonlinear numerical analysis of existing dam", *Archives of Civil Engineering*, **LIX**(1), pp. 21-49 (2013).

18. Hariri-Ardebili, M.A. and Mirzabozorg, H. "Numerical simulation of reservoir fluctuation effects on nonlinear dynamic response of concrete arch dams", *Advances in Fluid Mechanics VIII (AFM)*, WIT Press, Algarve, Portugal, pp. 427-438 (2010).

19. Hariri-Ardebili, M.A. and Mirzabozorg, H. "A comparative study of the seismic stability of coupled arch dam-foundation-reservoir systems using infinite elements and viscous boundary models", *International Journal of Structural Stability and Dynamic*, **13**(6), 24 pages, DOI: 10.1142/S0219455413500326 (2013).

20. Trifunac, M.D. and Brady, A.G. "A study of the duration of strong earthquake ground motion", *Bulletin of the Seismological Society of America*, **65**, pp. 581-626 (1975).

21. Hariri-Ardebili, M.A. and Mirzabozorg, H. "Effects of near-fault ground motions in seismic performance evaluation of a symmetry arch dam", *Soil Mechanics and Foundation Engineering*, **49**(5), pp. 192-199 (2012).

22. Bayraktar, A., Altunişik, A.C., Sevim, B., Kartal, M.E., Türker, T. and Bilici, Y. "Comparison of near- and far-fault ground motion effect on the nonlinear response of dam-reservoir-foundation systems", *Nonlinear Dynamic*, **58**, pp. 655-673 (2009).

23. Akköse, M. and Şimşek, E. "Non-linear seismic response of concrete gravity dams to near-fault ground motions including dam-water-sediment-foundation interaction", *Applied Mathematical Modelling*, **34**, pp. 3685-3700 (2010).

24. Bayraktar, A., Sevim, B., Altunışık, A.C., Türker, T., Kartal, M.E., Akköse, M. and Bilici, Y. et al. "Comparison of near and far fault ground motion effects on the seismic performance evaluation of dam-reservoir-foundation systems", *Dam Engineering*, **XIX**(4), pp. 201-239 (2009).

25. "EM 1110-2-6053, earthquake design and evaluation of concrete hydraulic structures", US Army Corps of Engineers, Washington D.C. (2007).

26. Ghanaat, Y. "Failure modes approach to safety evaluation of dams", *The 13th World Conference on Earthquake Engineering*, Vancouver, B.C., Canada (2004).

27. Hariri-Ardebili, M.A., Kolbadi, S.M., Heshmati, M. and Mirzabozorg, M. "Nonlinear analysis of concrete structural components using co-axial rotating smeared crack model", *Journal of Applied Science*, **12**(3), pp. 221-232 (2012).

Biographies

Mohammad Amin Hariri-Ardebili received BS and MS degrees in Civil Engineering from K.N. Toosi University of Technology, Tehran, Iran, in 2007 and 2010, respectively. He is currently pursuing his PhD degree in Structural Engineering and Mechanics at the University of Colorado, Boulder, USA. He was selected as distinguished graduate researcher of Civil Engineering Department of the K.N. Toosi University in 2010. His research interests include concrete dam engineering, advanced dynamic of structures and PBEE, and coupled system mechanics.

Hasan Mirzabozorg is Associate Professor of Civil Engineering at K.N. Toosi University of Technology, Tehran, Iran. His research interests include nonlinear seismic analysis of concrete dams, fluid-structure interaction, concrete fracture mechanics and alkali-aggregate reactions, and numerical methods in structural engineering. He regularly teaches "design of concrete dams", "finite element method" and "fracture mechanics".

Mohsen Ghaemian is Associate Professor in the Civil Engineering Department of Sharif University of Technology, Tehran, Iran. His research interests include dynamic responses of gravity and arch dams, especially dam-reservoir-foundation interaction effects, seismic response of dams due to non-uniform excitations and nonlinear behavior of concrete dams.